Materials Chemistry and Physics 194 (2017) 29–36

Contents lists available at ScienceDirect

Materials Chemistry and Physics

journal homepage: www.elsevier.com/locate/matchemphys

The study of structural and optical properties of (Eu, La, Sm) codoped ZnO nanoparticles via a chemical route

Jihui Lang [a], Qi Zhang [a], Qiang Han [a], Yue Fang [a], Jiaying Wang [a], Xiuyan Li [a], Yanqing Liu [a], Dandan Wang [b], Jinghai Yang [a, b, *]

[a] Key Laboratory of Functional Materials Physics and Chemistry of the Ministry of Education, Jilin Normal University, Siping, 136000, PR China
[b] Changchun Institute of Optics, Fine Mechanics and Physics, Chinese Academy of Sciences, Changchun, 130033, PR China

HIGHLIGHTS

- Doping of (Eu, La, Sm) ions into ZnO nanoparticles is realized by a chemical route.
- Eu^{3+}-related red emissions from intra-4f follow a similar trend as broad defect emission.
- Red emissions of Eu^{3+} enhance with RE codoping due to oxygen vacancies as energy storage centers.
- The bandgap can be tuned by RE codoping, which shows a prospect for the visible utilization.

GRAPHICAL ABSTRACT

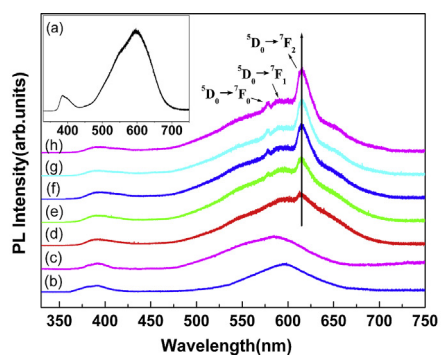

ARTICLE INFO

Article history:
Received 9 November 2016
Received in revised form
23 January 2017
Accepted 7 March 2017
Available online 19 March 2017

Keywords:
ZnO nanoparticles
RE ions codoping
Structural
Optical properties

ABSTRACT

The (Eu, La, Sm) ions were doped into ZnO nanoparticles by a chemical route, and the substitution of (Eu, La, Sm) for Zn^{2+} ions was proved by analytic techniques of X-ray diffraction (XRD), X-ray photoelectron spectroscopy (XPS), Raman, transmission electron microscope (TEM), photoluminescence (PL) and UV–vis absorption spectroscopy. The results revealed that the codoping did not change the wurtzite structure of ZnO nanoparticles, but the diameter of the nanoparticles decreased with increasing the rare earth (RE) doping concentrations. The optical bandgaps calculated through UV–visible absorption spectroscopy were found to decrease from 3.26 to 3.14 eV with increasing the RE doping concentrations, which also proved by the slight shift of UV positions in PL spectra. The sharp red emissions located at 578.2, 590.1 and 615.7 nm were originated from the 4f-4f transitions in Eu^{3+} ions under excitation of 325 nm. And these red emissions of Eu^{3+} ions showed a strong correlation with the energy storage centers of oxygen vacancies in the samples which was introduced by the other RE ions of La^{3+} and Sm^{3+} codoping.

1. Introduction

In recent years, considerable interest has been focused on ZnO nanomaterials due to its wide band gap and high exciton binding energy, as well as excellent optical, electronic and mechanical

* Corresponding author. Key Laboratory of Functional Materials Physics and Chemistry of the Ministry of Education, Jilin Normal University, Siping, 136000, PR China.
E-mail address: jhyang1@jlnu.edu.cn (J. Yang).

http://dx.doi.org/10.1016/j.matchemphys.2017.03.010
0254-0584/

properties. In most of these properties, it has been demonstrated to be applicable in ultraviolet luminescent or lasing devices [1–4]. However, it is highly desirable to achieve sharp visible emissions from ZnO nanomaterials for advanced display and lighting device applications such as distinguishable emissive flat panel display and LED backlights [5–7]. The chemical doping with suitable elements offers an effective method to enhance and control the structural, optical, electrical and magnetic properties of the nanomaterials. In particular, doping various RE elements such as Eu, Er, La, Sm, Ce etc in ZnO can modify their structural and optical properties significantly due to the intra-4f orbital transitions, which is crucial for their optical applications [8–11]. Various technologies such as magnetron sputtering, chemical bath deposition, pulsed laser deposition, hydrothermal, sol-gel, chemical vapor deposition and mechanical ball-milling method have been developed to synthesize the RE-doped ZnO nanomaterials. To date, the UV-excited emission of RE^{3+} ions can be observed, but it is relatively weak compared to the excitonic emission or defect emission from ZnO host, which may be due to the weak energy transfer between ZnO host and RE ions [12–14]. So, how to realize the energy transfer to enhance the UV-excited emission of RE^{3+} ions is an urgent issue. The codoping may be a useful way to overcome the mentioned problem.

The codoping can not only regulate the band structure, luminescence centers, defect sites or incorporate impurities for facilitating mobility of charge carriers simultaneously, but also provide a method for enhancing the optical performances in luminescent and catalytic materials by synergy effect of doping ions [15,16]. Among the RE ions, the Eu^{3+} ion is a representative RE ion for doping ZnO, and the Eu^{3+}-ralated red emissions can be used in light-emitting devices [8,9,14]. Sm^{3+} ion is also one of the RE ions, which has the ability to shift the band gap of ZnO into visible region and to control electron-hole recombination [17]. And La^{3+} ion with the largest ionic radius among the RE ions perhaps has the strong power to change the structure and introduce the more defect sites in ZnO host. So the codoping of (Eu, La, Sm) into ZnO is a meaningful work, which may enhance the RE-related visible emissions and expands band gap of ZnO host at the same time. According to the recent literature, the reports about the RE doped ZnO nanomaterials mainly focus on the single RE ion doping, and about the codoping with more than two RE ions is limited. Hence, more attention should be paid onto the codoped ZnO systems.

In this paper, the (Eu, La, Sm) codoped ZnO nanoparticles with various doping concentrations have been synthesized via a chemical precipitation route, and the incorporation, morphologies and optical properties of the nanoparticles are studied in detail. The doping concentrations of RE photoluminescence have been analyzed, which indicates that carrier-mediated acted as the energy storage centers play an important role in the energy transfer process.

2. Experimental

In the experiment, the codoped samples were synthesized by the chemical precipitation method. The zinc nitrate hexahydrate ($Zn(NO_3)_2 \cdot 6H_2O$), europium oxide (Eu_2O_3), lanthanum oxide (La_2O_3), samarium oxide (Sm_2O_3) and ammonium bicarbonate (NH_4HCO_3) were used as the starting materials without further purification. First, the appropriated amounts of $Zn(NO_3)_2 \cdot 6H_2O$ was dissolved in deionized water, and the rare earth nitrates of $Eu(NO_3)_3$, $La(NO_3)_3$ and $Sm(NO_3)_3$ were prepared by dissolving the REO of Eu_2O_3, La_2O_3 and Sm_2O_3 in concentrated nitric acid, respectively. Second, the two solutions were mixed with different molar ratio of Zn^{2+}/RE^{3+}(Eu^{3+}, La^{3+}, Sm^{3+}), and the appropriated amounts of NH_4HCO_3 was slowly dropped into the above solutions. The mixed solutions were stirred for 2 h at room temperature (RT). Subsequently, the white precipitates were formed and collected. Then, the white precipitates washed with alcohol for several times were dried at 60 °C for 4 h. Finally, the products were calcined at 400 °C for 2 h in air atmosphere [18,19].

The structural characterization of the codoped samples was performed on a D/max-RA XRD spectrometer with a Cu Kα line operated at 40 kV (λ = 0.15406 nm MAC Science, MXP18, Japan). The morphologies and compositional analysis of the samples were examined by transition electron microscopy at the accelerating voltage of 200 kV (TEM, JEM-2010HR, Japan) and X-ray photoelectron spectroscopy via Al Kα line with a photon-energy of 1486.6 eV (XPS, VG-ESCALAB Mark II UK, resolution: 0.5 eV). The optical properties were obtained by RT photoluminescence spectra using a continuous He–Cd laser with a wavelength of 325 nm at 50 mW (PL, Renishaw-inVia) and UV–vis absorption spectra using UV–Vis spectrophotometer of UV-5800PC in the wavelength range of 190–1100 nm (Shanghai Metash Instruments Co., Ltd). Raman spectra were obtained using the 514 nm line of an argon ion laser at an incident power of 20 mW (Renishaw-inVia, resolution: 1–2 cm^{-1}).

3. Results and discussion

Fig. 1 shows the XRD patterns of pure ZnO, $Zn_{0.95}Eu_{0.05}O$, $Zn_{0.97}Sm_{0.03}O$, $Zn_{0.97}La_{0.03}O$ and $Zn_{0.92-x}Eu_{0.05}Sm_{0.03}La_xO$ samples (x = 0, 0.01, 0.02 and 0.03). These samples are named as sample A to sample H, respectively. All the diffraction peaks can be indexed to a hexagonal wurtzite structured ZnO, which coincides with the standard JCPDS cards (No. 36-1451) [20]. The lattice parameters of these samples are obtained by fitting the XRD data with the least square method (LSM), and the results can be seen in Table 1. It is found that the lattice parameters of doped ZnO are a little larger than that of pure one. The increased lattice parameters indicate that the RE ions of Eu^{3+}, Sm^{3+} and La^{3+} may be doped into the ZnO crystal lattice via the substitution of the Zn^{2+} sites because of the large difference in ionic radius between the Zn^{2+} and RE^{3+} [21,22]. The average size D is calculated using Scherrer formula, which can be described as follows:

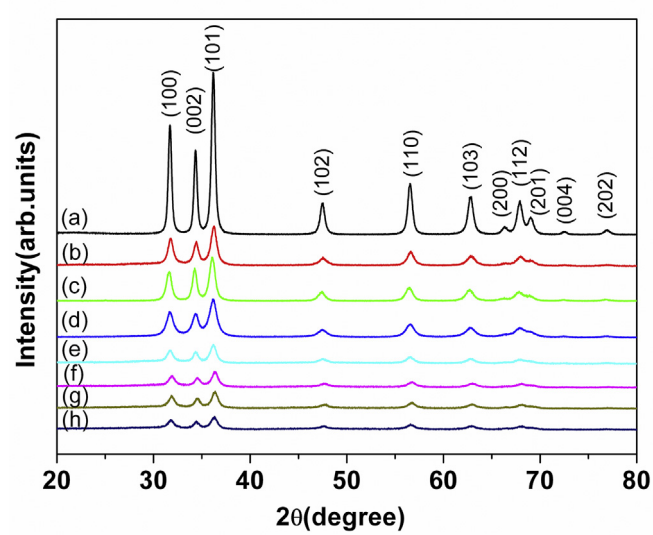

Fig. 1. XRD patterns of pure ZnO (a), $Zn_{0.95}Eu_{0.05}O$ (b), $Zn_{0.97}Sm_{0.03}O$ (c), $Zn_{0.97}La_{0.03}O$ (d) and $Zn_{0.92-x}Eu_{0.05}Sm_{0.03}La_xO$ samples (e) x = 0, (f) x = 0.01, (g) x = 0.02, (h) x = 0.03.

Table 1
The calculated results from XRD data.

Sample	a(Å)[a]	c(Å)[a]	Average size (nm)
A	3.2411	5.2017	32.0
B	3.2431	5.2074	25.7
C	3.2432	5.2080	25.4
D	3.2483	5.2083	24.6
E	3.2488	5.2100	23.8
F	3.2534	5.2146	21.5
G	3.2553	5.2159	14.2
H	3.2554	5.2211	9.0

[a] Corresponding errors of lattice parameters <0.001.

$$D = 0.89\lambda/\beta \cos\theta \quad (1)$$

where λ is the X-ray wavelength, β is the full width at half maximum (FWHM) and θ is the maximum of the Bragg diffraction peak. From Table 1, the average size of sample A to sample H, calculated for the peak (101), is about 32.0, 25.7, 25.4, 24.6, 23.8, 21.5, 14.2 and 9.0 nm, respectively. The decreased size of these samples can be further proved by TEM images. Fig. 2 shows the TEM images of pure ZnO, $Zn_{0.95}Eu_{0.05}O$, $Zn_{0.92}Eu_{0.05}Sm_{0.03}O$ and $Zn_{0.89}Eu_{0.05}Sm_{0.03}La_{0.03}O$ samples. The TEM image of pure ZnO exhibits the rounded particles with average size of 25 nm (Fig. 2

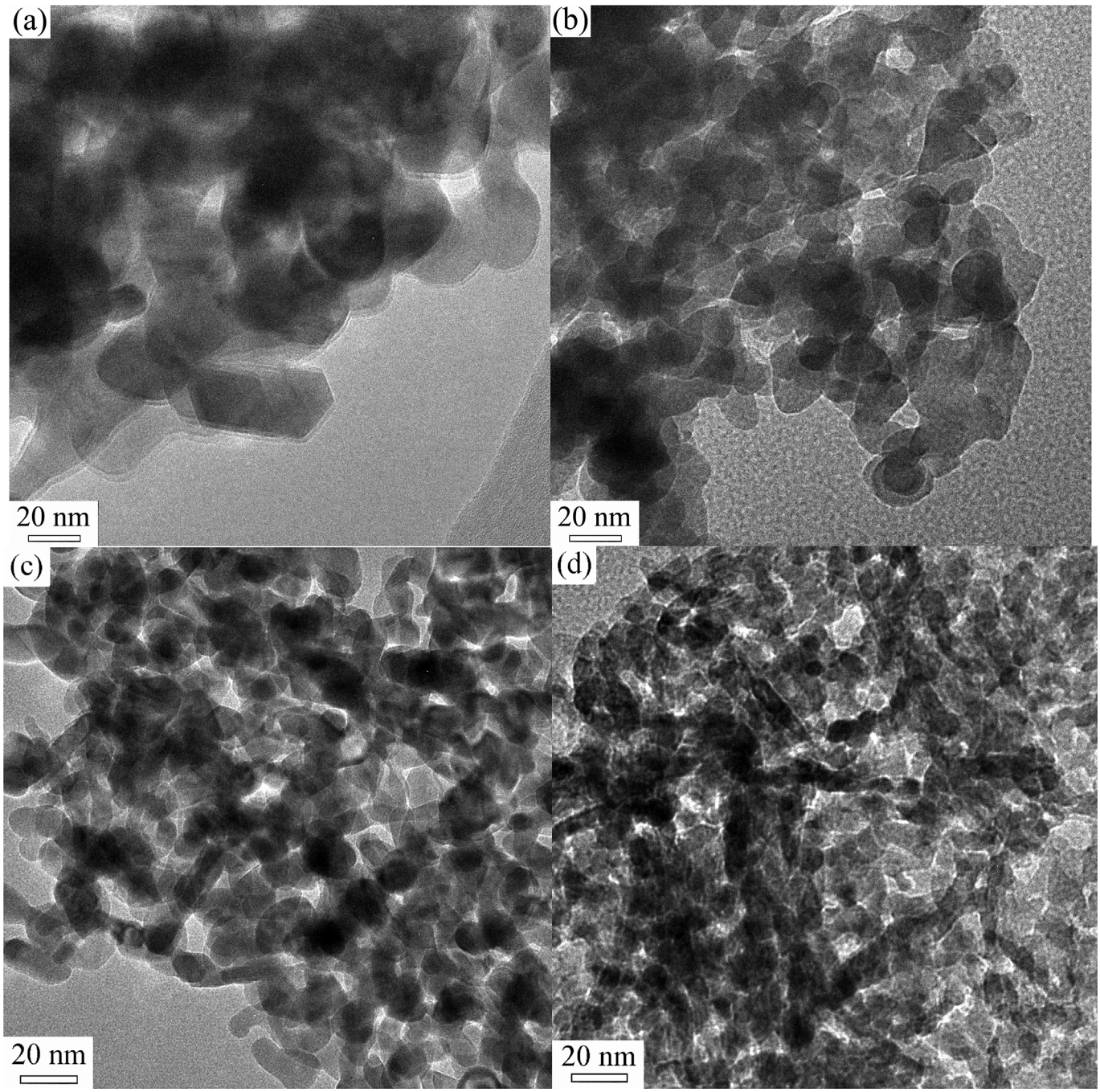

Fig. 2. TEM images of pure ZnO (a), $Zn_{0.95}Eu_{0.05}O$ (b), $Zn_{0.92}Eu_{0.05}Sm_{0.03}O$ (c) and $Zn_{0.89}Eu_{0.05}Sm_{0.03}La_{0.03}O$ (d) samples.

(a)). Compared to the pure ZnO, the increase in RE (Eu^{3+}, La^{3+}, Sm^{3+}) doping concentrations does not induce obvious change in morphology of nanoparticle. But the average particle size of ZnO samples decreases from 25 to 7 nm as increasing the doping concentrations of RE (Eu^{3+}, La^{3+}, Sm^{3+}), which exhibits a good agreement with the XRD results. The average particle size of these samples decreases as increasing the RE doping concentrations, which could be attributed to the interference of the RE ions to the ZnO crystal growth. It can be explained as follows. The chemical precipitation method we used contains two growth processes including the precipitation formation and the calcination treatment. In the process of precipitation formation, the Zn-O-RE nuclei will be formed when the RE ions are doped into the ZnO host. However, the nucleation rate will be restrained at the nucleation

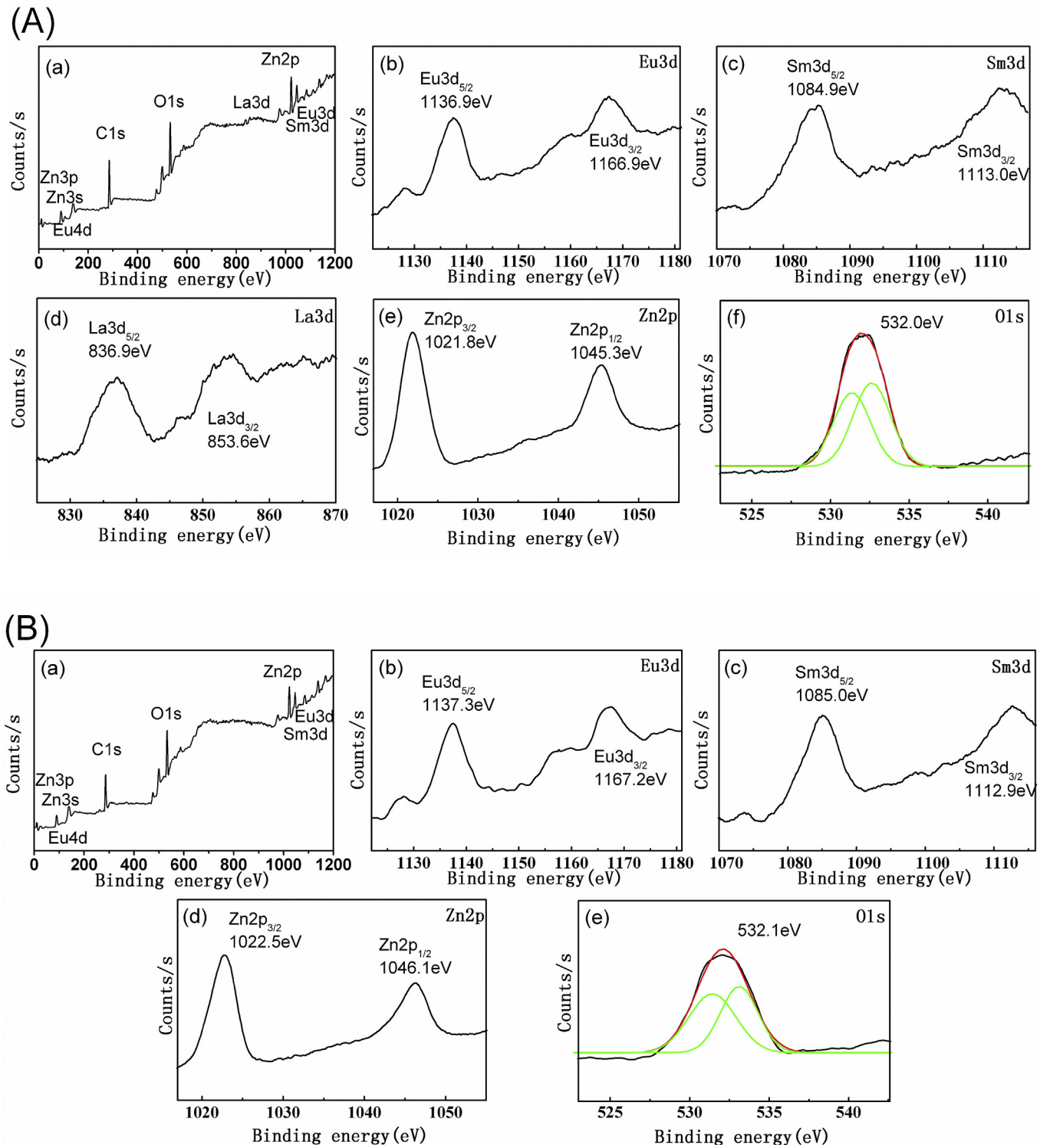

Fig. 3. XPS spectra of $Zn_{0.90}Eu_{0.05}Sm_{0.03}La_{0.02}O$ (A) and $Zn_{0.92}Eu_{0.05}Sm_{0.03}O$ (B) samples.

process due to the large differences in ionic radius and valence state between RE^{3+} and Zn^{2+} ions. And then in the calcination treatment, some RE ions locating in the interfaces or grain boundaries between nanoparticles might substitute into the Zn^{2+} sites to lower the interfacial energy of the nanoparticles, which are combined one single nanocrystal with two or more ZnO nanoparticles in the crystallization process. That is to say, the obstructions for the movement of grain boundary and restriction of the subsequent grain growth will be appeared by the interference of RE ions. So, it is believed that the formation of Zn-O-RE in the crystal lattice and the large difference between RE^{3+} and Zn^{2+} ions are the main reasons for the decreased size with RE codoping in our case. The above result has a good agreement with our previous reports [23,24], wherein we testified that the size could decrease with doping of Y^{3+} and La^{3+} in ZnO nanomaterials respectively.

Fig. 3A shows the XPS spectrum of $Zn_{0.90}Eu_{0.05}Sm_{0.03}La_{0.02}O$ sample. The binding energies are calibrated using the carbon peak (C1s) at 285.0 eV as reference. As shown in the survey XPS spectrum, all of the peaks can be ascribed to Zn, Eu, La, Sm, O and C elements as labeled in Fig. 3A(a). It indicates that there are no other impurities in $Zn_{0.90}Eu_{0.05}Sm_{0.03}La_{0.02}O$ sample, which shows a good agreement with the above XRD results. The binding energies of Zn2p3/2 and Zn2p1/2 in Fig. 3A(e) are located at 1021.0 and 1045.2 eV, which agrees well with the standard value of Zn^{2+} ions in the oxide [25,26]. The O1s signal in Fig. 3A(f) can be fitted into two peaks, indicating that at least two different kinds of O species in the surface of $Zn_{0.90}Eu_{0.05}Sm_{0.03}La_{0.02}O$ sample. As reported in the literature, the two peaks located at 531.3 and 532.5 eV can be attributed to the lattice oxygen in a metallic oxides, oxygen of surface hydroxyl or chemisorbed oxygen, respectively [19,27,28]. Besides the strong signals of Zn and O, the peaks corresponding to Eu3d, Sm3d and La3d core levels are observed as well. The two peaks located at 1135.2 and 1164.6 eV can be assigned to Eu3d5/2 and Eu3d3/2 core levels (Fig. 3A(b)), which indicate that the Eu ion has the trivalent valance state in codoped sample [29,30]. The peaks located at 1084.6 and 1112.8 eV are corresponding to Sm3d5/2 and Sm3d3/2 core levels (Fig. 3A(c)), and the peak positions confirm the existence of Sm ions in trivalent valence state [31]. The La3d5/2 and La3d3/2 core levels shown in Fig. 3A(d) also reveal that the La ions exist in the form of trivalent valence in the codoped sample [32,33]. For comparison, the XPS spectrum of $Zn_{0.92}Eu_{0.05}Sm_{0.03}O$ sample is also given in Fig. 3B. The appearance of (Eu, Sm) peaks and their positions illustrate that the Eu and Sm ions are both trivalent valance state in this sample. According to the two XPS results and above analysis, the valence states of RE ions do not changed with La doping in our case. Moreover, the Eu: Sm: Zn ratio of $Zn_{0.92}Eu_{0.05}Sm_{0.03}O$ sample is determined from XPS data to be 0.044: 0.026: 0.930 and the Eu: Sm: La: Zn ratio of $Zn_{0.90}Eu_{0.05}Sm_{0.03}La_{0.02}O$ sample is determined to be 0.044: 0.025: 0.015: 0.916, which are close to the proposed doping concentrations. Combined with the XRD results, the above analysis testifies that the RE dopants are incorporated into ZnO lattice.

Raman scattering is a useful technique to investigate the microstructure of nanomaterials. Fig. 4 shows the RT Raman spectra of sample A to sample H with the 514 nm line of an argon laser. The peaks located at 330, 377, 438 and 580 cm^{-1} can be assigned to E_{2H}-E_{2L}, $A_{1(TO)}$, E_{2H} and $A_{1(LO)}$ vibration modes of ZnO with $P6_3mc$ symmetry [34–37]. The strongest peak centered at about 438 cm^{-1} can be observed in all the Raman spectra, and the intensity of this peak decreases with increasing the RE doping concentrations. It may be mainly related with the worse crystallization of the codoped samples due to the distortion of the crystal lattice in ZnO by RE codoping [33,38–40]. Moreover, the sample absorption may be another reason for the decrease of the Raman peaks. The broadened and weak peak at 580 cm^{-1} appeared in the

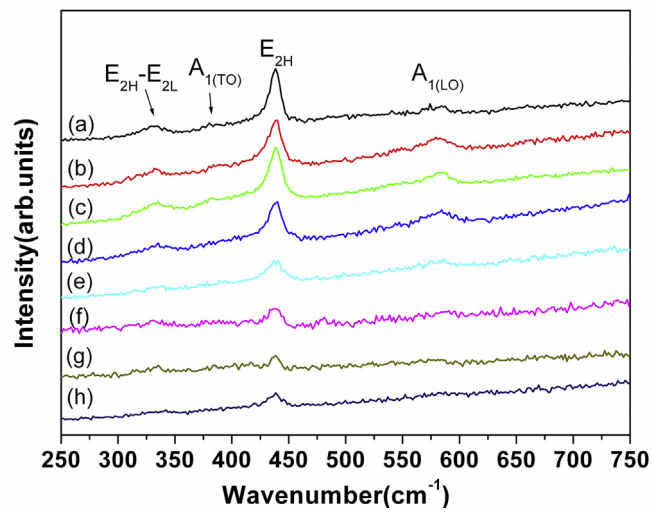

Fig. 4. Raman spectra of pure ZnO (a), $Zn_{0.95}Eu_{0.05}O$ (b), $Zn_{0.97}Sm_{0.03}O$ (c), $Zn_{0.97}La_{0.03}O$ (d) and $Zn_{0.92-x}Eu_{0.05}Sm_{0.03}La_xO$ samples (e) x = 0, (f) x = 0.01, (g) x = 0.02, (h) x = 0.03.

spectra is usually related with the defects of O-vacancy, Zn-interstitial or their complexes, indicating some defects exist in our samples [41,42]. And the appearance of the other modes E_{2H}-E_{2L} and $A_{1(TO)}$ further proves the dominant characters of the wurtzite phase in the samples. The above analysis implies the synthesis of (Eu^{3+}, La^{3+}, Sm^{3+}) codoped ZnO samples with wurtzite phase by a chemical route.

Fig. 5 shows the RT PL spectra of sample A to sample H. Under UV light of 325 nm, the sample A (pure ZnO) in Fig. 5 (a) shows a weak UV emission due to the recombination of the free excitons in ZnO and a strong broad visible emission originated from the deep level defect state of ZnO. As seen in Fig. 5, it can be seen that the positions of UV emission from sample A to sample H are located at 386.4, 388.9, 389.7, 390.4, 391.3, 393.3, 393.5 and 394.5 nm, respectively. Obviously, a red shift of UV emission appears in our codoped samples, illustrating the bandgap of these samples become narrowed with increasing the doping concentrations of Eu^{3+}, La^{3+} and Sm^{3+}. We present the UV–vis absorption spectra in Fig. 6 and calculate the optical bandgap E_g of these samples using

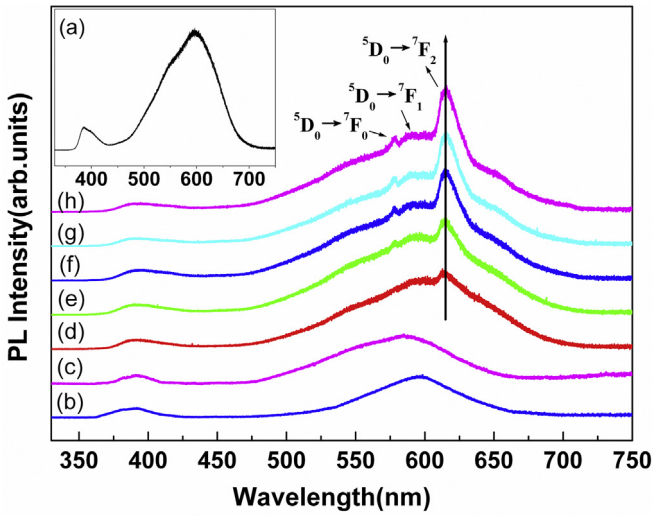

Fig. 5. PL spectra of pure ZnO (a), $Zn_{0.95}Eu_{0.05}O$ (b), $Zn_{0.97}Sm_{0.03}O$ (c), $Zn_{0.97}La_{0.03}O$ (d) and $Zn_{0.92-x}Eu_{0.05}Sm_{0.03}La_xO$ samples (e) x = 0, (f) x = 0.01, (g) x = 0.02, (h) x = 0.03.

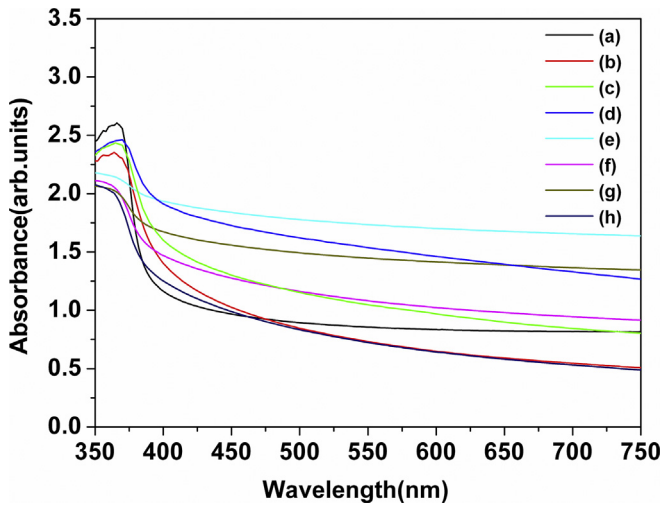

Fig. 6. UV–Vis absorption spectra of pure ZnO (a), $Zn_{0.95}Eu_{0.05}O$ (b), $Zn_{0.97}Sm_{0.03}O$ (c), $Zn_{0.97}La_{0.03}O$ (d) and $Zn_{0.92-x}Eu_{0.05}Sm_{0.03}La_xO$ samples (e) x = 0, (f) x = 0.01, (g) x = 0.02, (h) x = 0.03.

the Tauc relation of $\alpha = A(h\nu - E_g)^n/h\nu$, where A is a constant, α is the absorption coefficient that calculated by Lambert-Beer Law and n is a constant of 1/2 for the direct bandgap semiconductor [43]. The values of E_g are calculated by plotting Tauc's graphs between $(\alpha h\nu)^2$ versus $h\nu$ and the intercept of this linear region on the energy axis at $(\alpha h\nu)^2$ equal to zero gives the bandgap. The estimated bandgaps of sample A to sample H are presented in Fig. 7. We can see that the value of $E_g$decreases from 3.26 eV (sample A) to a minimum value of 3.14 eV (sample H). The narrowing of the bandgaps with RE (Eu^{3+}, La^{3+}, Sm^{3+}) codoping is mainly due to two effects of the new impurity bands introducing by RE ions and the strong orbital coupling between RE and O [23,38,44,45]. First, the codoping of RE ions (Eu^{3+}, La^{3+}, Sm^{3+}) will introduce the additional electron states of impurity bands and they will locate closer to the lower edge of the conduction band to form the new lowest unoccupied molecular orbital. This phenomenon is the main reason for the reduction of the band gap and eventually makes the red shift of UV emission. Second, the RE substitution also lead the strong sp-d exchange interactions between the band electrons and the localized d electrons of the RE ions which substitute Zn^{2+} ions. The s-d and p-d exchange interactions lead to a negative and a positive correction to the conduction band and the valence band edges separately, resulting in the bandgap narrowing and red shift of UV emission. Similar results have been obtained in our previous studies [23,38].

In addition, a strong broad visible emission appeared in all the spectra is also analyzed. It is important to note that the sharp red emissions superimposed on the broad defect-related PL are observed in the doped samples except sample B and C, and the intensity of these red emissions gradually enhances with increasing the RE doping concentrations. The red emissions centered at 578.2, 590.1 and 615.7 nm can be attributed to the $^5D_0 \rightarrow {}^7F_0$, $^5D_0 \rightarrow {}^7F_1$ and $^5D_0 \rightarrow {}^7F_2$ transitions of the Eu^{3+} ions in our case, respectively [46–48]. As we known, the Eu^{3+} ions are usually incorporated in ZnO by substitution on the metal sublattice with C_{3v} site symmetry which splits ground $^7F_{2\text{-}5}$ levels. And the intensity ratio of $^5D_0 \rightarrow {}^7F_2$ transition to $^5D_0 \rightarrow {}^7F_1$ transition might provide structural

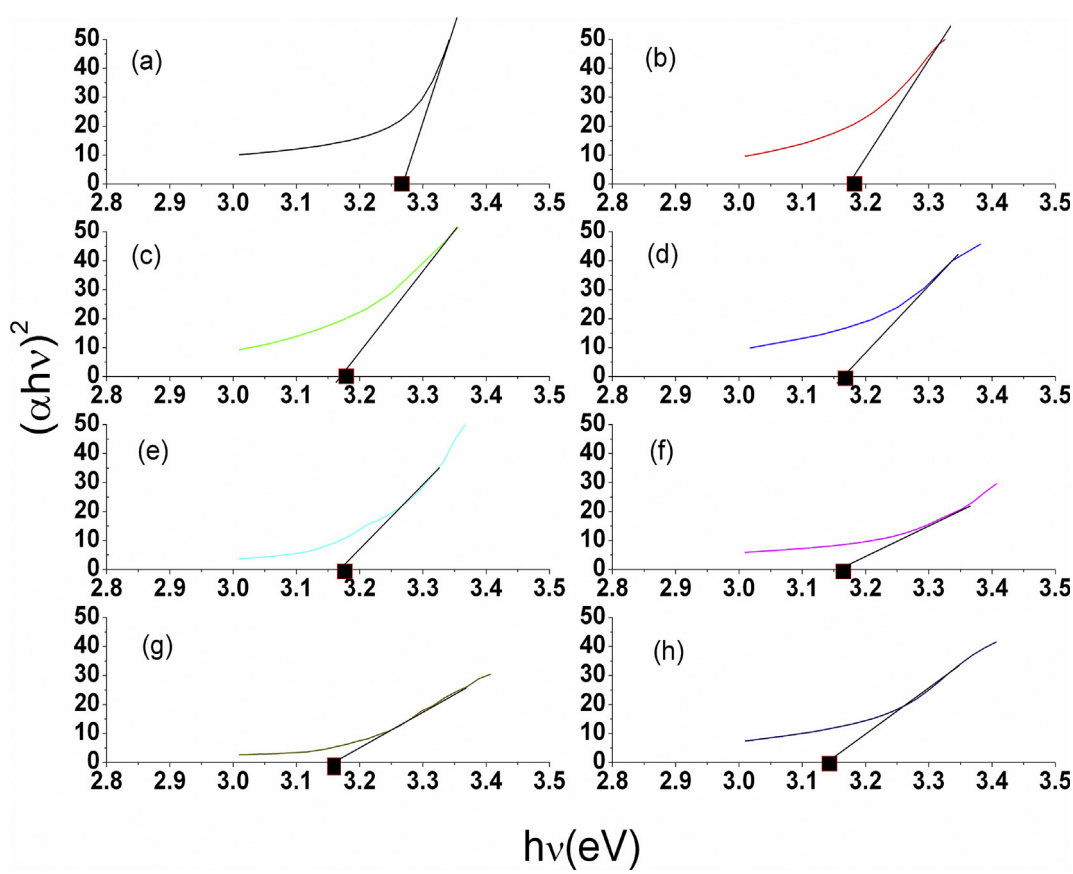

Fig. 7. Relation curves of $(\alpha h\nu)^2$ versus $h\nu$ of pure ZnO (a), $Zn_{0.95}Eu_{0.05}O$ (b), $Zn_{0.97}Sm_{0.03}O$ (c), $Zn_{0.97}La_{0.03}O$ (d) and $Zn_{0.92-x}Eu_{0.05}Sm_{0.03}La_xO$ samples (e) x = 0, (f) x = 0.01, (g) x = 0.02, (h) x = 0.03.

information such as distortion of the ligand environment and site symmetry. Based on the above analysis, the stronger ratio of $^5D_0 \rightarrow {}^7F_2$ to $^5D_0 \rightarrow {}^7F_1$ appeared in our spectra illustrates that the Eu^{3+} ions are incorporated into ZnO lattice by substitution on the Zn sublattice and located at a low-symmetry site (C_{3v}) without inversion center. Compared with the doped and codoped samples, it is found that the red emissions of Eu^{3+} enhance with increasing the other RE doping concentrations of La^{3+} and Sm^{3+}. The above results reveal that the Eu^{3+} ions can act as luminescent centers in ZnO nanoparticles and also provides an efficient pathway for carrier-mediated excitation of Eu^{3+} ions. According to our previous work, the defect of singly ionized oxygen vacancies can act as the energy storage centers that mediate the energy transfer from the ZnO host to the Eu^{3+} ions [14,18,49]. That is to say, there is a strong correlation between the red emissions of Eu^{3+} and the defect of singly ionized oxygen vacancies. Based on our PL spectra, the broad visible emission centered at about 570 nm are mainly attributed to oxygen vacancies and this emission gradually enhances as increasing the RE doping concentrations. It indicates that the numbers of the oxygen vacancies including singly ionized oxygen vacancies are increased with further increasing the other RE doping concentrations of La^{3+} and Sm^{3+}, which eventually makes the enhancement of the red emissions of Eu^{3+}. In addition, no obvious characteristic emissions of the La^{3+} and Sm^{3+} appears in the spectra due to the weak energy transfer between the two ions and ZnO, but the codoping can introduce more oxygen vacancies as the energy storage centers, which can assist the energy transfer process from ZnO host to Eu^{3+} ions.

4. Conclusion

The present work studies the structural and optical properties of (Eu, La, Sm) codoped ZnO nanoparticles prepared via a chemical route. Structural analysis of the nanocrystals shows the formation of nanosized (Eu, La, Sm) codoped ZnO particles with uniform size, and the size of these samples changes from 25 nm to 7 nm as increasing the RE doping concentrations. From the optical analysis, a mechanism has been proposed, which involve energy transfer occur from ZnO host to Eu^{3+} ions by defect-mediated as the energy storage centers. The codoping of the other RE ions can further raise the defect-mediated in this energy transfer, so that the red characteristic emissions are eventually enhanced in the codoped ZnO nanoparticles. Moreover, the interesting optical analysis show that the bandgap of these samples decreases due to the RE codoping. All above obtained results encourage people to further design ZnO nanostructures with codoping the other elements, which is beneficial for extending their promising application in optical fields.

Acknowledgements

This work is supported by the National Natural Science Foundation of China (Grant Nos. 51608226, 11254001, 21576111), Program for New Century Excellent Talents in University (Item No. NCET-13-0824), Program for the development of Science and Technology of Jilin Province (Item No. 20140101205JC) and Program for the development of Science and Technology of Siping City (Item No. 2015065).

References

[1] Z.K. Tang, G.K.L. Wong, P. Yu, Y. Segawa, Room-temperature ultraviolet laser emission from self-assembled ZnO microcrystallite thin films, Appl. Phys. Lett. 72 (1998) 3270–3272.
[2] M.H. Huang, S. Mao, H. Feick, H.Q. Yan, Y.Y. Wu, H. Kind, E. Weber, R. Russo, P.D. Yang, Room-temperature ultraviolet nanowire nanolasers, Science 292 (2001) 1897–1899.
[3] Y.K. Su, S.M. Peng, L.W. Ji, C.Z. Wu, W.B. Cheng, C.H. Liu, Ultraviolet ZnO nanorod photosensors, Langmuir 26 (2010) 603–606.
[4] A. Al-Nafiey, B. Sieber, B. Gelloz, A. Addad, M. Moreau, J. Barjon, M. Girleanu, O. Ersen, R. Boukherroub, Enhanced ultraviolet luminescence of ZnO nanorods treated by high-pressure water vapor annealing (HWA), J. Phys. Chem. C 120 (2016) 4571–4580.
[5] C.T. Lee, Fabrication methods and luminescent properties of ZnO materials for light-emitting diodes, Materials 3 (2010) 2218–2259.
[6] S. Chawla, M. Saroha, R.K. Kotnala, White light emitting magnetic ZnO: Sm nanoparticles prepared by inclusive co-precipitation synthesis, Electron. Mater. Lett. 10 (2014) 73–80.
[7] H.H. Huang, C.C. Dun, W.X. Huang, Y. Cui, J.W. Xu, Q.K. Jiang, C.W. Xu, H. Zhang, S.C. Wen, D.L. Carroll, Solution-processed yellow-white light-emitting diodes based on mixed-solvent dispersed luminescent ZnO nanocrystals, Appl. Phys. Lett. 106 (1–5) (2015) 263506.
[8] D.D. Wang, G.Z. Xing, M. Gao, L.L. Yang, J.H. Yang, T. Wu, Defects-mediated energy transfer in red-light-emitting Eu-doped ZnO nanowire arrays, J. Phys. Chem. C 115 (2011) 22729–22735.
[9] L. Luo, F.Y. Huang, G.S. Dong, Y.H. Wang, Z.F. Hu, J. Chen, White light emission and luminescence dynamics in Eu^{3+}/Dy^{3+} codoped ZnO nanocrystals, J. Nanosci. Nanotechnol. 16 (2016) 619–625.
[10] S. Bishnoi, N. Khichar, R. Das, V. Kumar, R.K. Kotnala, S. Chawla, Triple excitation with dual emission in paramagnetic ZnO: Er^{3+} nanocrystals, RSC Adv. 4 (2014) 32726–32729.
[11] W.M. Jadwisienczak, H.J. Lozykowski, A. Xu, B. Patel, Visible emission from ZnO doped with rare-earth ions, J. Electron. Mater. 31 (2002) 776–784.
[12] S. Bachir, K. Azuma, J. Kossanyi, P. Valet, J.C. Ronfard-Haret, Photoluminescence of polycrystalline zinc oxide co-activated with trivalent rare earth ions and lithium. Insertion of rare-earth ions into zinc oxide, J. Lumin 75 (1997) 35–49.
[13] Q.T. Tang, H.L. Shen, J. Jiao, W.L. Chen, ZnO: Er, Li film prepared by sol-gel method and its properties of converting both UV and NIR light to visible light, Opt. Mater. 39 (2015) 218–223.
[14] J.H. Yang, X. Li, J.H. Lang, L.L. Yang, M. Gao, X.Y. Liu, M.B. Wei, Y. Liu, R. Wang, Effects of mineralizing agent on the morphologies and photoluminescence properties of Eu^{3+}-doped ZnO nanomaterials, J. Alloy. Compd. 509 (2011) 10025–10031.
[15] C. Li, R.S. Hu, T.T. Zhou, H.T. Wu, K.P. Song, X.X. Liu, R.D. Wang, Special morphologies of Mg, Ca, and Y-doped ZnO/La_2O_3 composite for photocatalysis, Mater. Lett. 124 (2014) 81–84.
[16] N. Kaneva, A. Bojinova, K. Papazova, D. Dimitrov, Photocatalytic purification of dye contaminated sea water by lanthanide ($La^{3}+$, Ce^{3+}, Eu^{3+}) modified ZnO, Catal. Today 252 (2015) 113–119.
[17] J.C. Sin, S.M. Lam, K.T. Lee, A.R. Mohamed, Preparation and photocatalytic properties of visible light-driven samarium-doped ZnO nanorods, Ceram. Int. 39 (2013) 5833–5843.
[18] J.H. Lang, Q. Han, X. Li, S.S. Xu, J.H. Yang, L.L. Yang, Y.S. Yan, X.Y. Li, Y.S. Sui, X.Y. Liu, J. Cao, J. Wang, Effect of annealing temperature on the energy transfer in Eu-doped ZnO nanoparticles by chemical precipitation method, J. Mater. Sci. Mater. Electron 24 (2013) 4542–4548.
[19] J.H. Lang, J.Y. Wang, Q. Zhang, X.Y. Li, Q. Han, M.B. Wei, Y.R. Sui, D.D. Wang, J.H. Yang, Chemical precipitation synthesis and significant enhancement in photocatalytic activity of Ce-doped ZnO nanoparticles, Ceram. Int. 42 (2016) 14175–14181.
[20] T.K. Jia, W.M. Wang, F. Long, Z.Y. Fu, H. Wang, Q.J. Zhang, Fabrication, characterization and photocatalytic activity of La-doped ZnO nanowires, J. Alloy. Compd. 484 (2009) 410–415.
[21] K. Ueda, H. Tabata, T. Kawai, Magnetic and electric properties of transition-metal-doped ZnO films, Appl. Phys. Lett. 79 (2001) 988–990.
[22] J.H. Yang, X. Li, J.H. Lang, L.L. Yang, M.B. Wei, M. Gao, X.Y. Liu, H.J. Zhai, R. Wang, Y. Liu, J. Cao, Synthesis and optical properties of Eu-doped ZnO nanosheets by hydrothermal method, Mat. Sci. Semicon. Proc. 14 (2011) 247–252.
[23] J.H. Lang, Y. Fang, Q. Zhang, J.Y. Wang, T.S. Li, X.Y. Li, Q. Han, D.D. Wang, M.B. Wei, J.H. Yang, Synthesis, characterization and photoluminescence property of La-doped ZnO nanoparticles, Appl. Phys. A 122 (1–7) (2016) 873.
[24] J.H. Yang, R. Wang, L.L. Yang, J.H. Lang, M.B. Wei, M. Gao, X.Y. Liu, J. Cao, X. Li, N.N. Yang, Tunable deep-level emission in ZnO nanoparticles via yttrium doping, J. Alloy. Compd. 509 (2011) 3606–3612.
[25] B. Chouchene, T.B. Chaabane, L. Balan, E. Girot, K. Mozet, G. Medjahdi, R. Schneider, High performance Ce-doped ZnO nanorods for sunlight-driven photocatalysis, Beilstein J. Nanotechnol. 7 (2016) 1338–1349.
[26] G.R. Li, X.H. Lu, W.X. Zhao, C.Y. Su, Y.X. Tong, Controllable electrochemical synthesis of Ce^{4+}-doped ZnO nanostructures from nanotubes to nanorods and nanocages, Cryst. Growth Des. 8 (2008) 1277–1281.
[27] L. Armelao, D. Barreca, G. Bottaro, A. Gasparotto, D. Leonarduzzi, C. Maragno, E. Tondello, C. Sada, Tailored synthesis of ZnO: Er(III) nanosystems by a hybrid rf-sputtering/sol-gel route, J. Vac. Sci. Technol. A 24 (2006) 1941–1947.
[28] Y.Y. Zhang, Q.L. Wang, J. Xu, S.Y. Ma, Synthesis of Pd/ZnO nanocomposites with high photocatalytic performance by a solvothermal method, Appl. Surf. Sci. 258 (2012) 10104–10109.
[29] A. Oudhia, N. Shukla, P. Bose, R. Lalwani, A. Choudhary, Effect of various synthesis protocols on doping profile of ZnO: Eu Nanowires, Nano-Struct. Nano-Objects 7 (2016) 69–74.
[30] K. Suzuki, K. Murayama, N. Tanaka, Enhanced luminescence in Eu-doped ZnO

nanocrystalline films, Appl. Phys. Lett. 107 (1–4) (2015) 031902.
[31] G.S. Thool, M. Arunakumari, A.K. Singh, S.P. Singh, Shape tunable synthesis of Eu- and Sm-doped ZnO microstructures: a morphological evaluation, Bull. Mater. Sci. 38 (2015) 1519–1525.
[32] S. Anandan, A. Vinu, K.L.P. Sheeja Lovely, N. Gokulakrishnan, P. Srinivasu, T. Mori, V. Murugesan, V. Sivamurugan, K. Ariga, Photocatalytic activity of La-doped ZnO for the degradation of monocrotophos in aqueous suspension, J. Mol. Catal. A Chem. 266 (2007) 149–157.
[33] H.D. Zhang, M. Yu, J.C. Zhang, C.H. Sheng, X. Yan, W.P. Han, Y.C. Liu, S. Chen, G.Z. Shen, Y.Z. Long, Fabrication and photoelectric properties of La-doped p-type ZnO nanofibers and crossed p-n homojunctions by electrospinning, Nanoscale 7 (2015) 10513–10518.
[34] G. Xiong, U. Pal, J. Garcia Serrano, Correlations among size, defects, and photoluminescence in ZnO nanoparticles, J. Appl. Phys. 101 (1–6) (2007) 024317.
[35] L.L. Yang, J.H. Yang, D.D. Wang, Y.J. Zhang, Y.X. Wang, H.L. Liu, H.G. Fan, J.H. Lang, Photoluminescence and Raman analysis of ZnO nanowires deposited on Si (100) via vapor–liquid–solid process, Phys. E 40 (2008) 920–923.
[36] A. Kovalenko, G. Pourroy, O. Crégut, M. Gallart, B. Hönerlage, P. Gilliot, Evidence of unintentional n-doping in ZnO nanorods, J. Phys. Chem. C 114 (2010) 9498–9502.
[37] J.H. Lang, J.Y. Wang, Q. Zhang, S.S. Xu, D.L. Han, J.H. Yang, Q. Han, L.L. Yang, Y.R. Sui, X.Y. Li, X.Y. Liu, Synthesis and photoluminescence characterizations of the Er^{3+}-doped ZnO nanosheets with irregular porous microstructure, Mat. Sci. Semicon. Proc. 41 (2016) 32–37.
[38] J.H. Lang, Q. Han, J.H. Yang, C.S. Li, X. Li, L.L. Yang, Y.J. Zhang, M. Gao, D.D. Wang, J. Cao, Fabrication and optical properties of Ce-doped ZnO nanorods, J. Appl. Phys. 107 (1–4) (2010) 074302.
[39] Gugu H. Mhlongo, David E. Motaung, Steven S. Nkosi, H.C. Swart, Gerald F. Malgas, Kenneth T. Hillie, Bonex W. Mwakikunga, Temperature-dependence on the structural, optical, and paramagnetic properties of ZnO nanostructures, Appl. Surf. Sci. 293 (2014) 62–70.
[40] J.H. Lang, Q. Han, C.S. Li, J.H. Yang, X. Li, L.L. Yang, D.D. Wang, H.J. Zhai, M. Gao, Y.J. Zhang, X.Y. Liu, M.B. Wei, Effect of Mn doping on the microstructures and photoluminescence properties of CBD derived ZnO nanorods, Appl. Surf. Sci. 256 (2010) 3365–3368.
[41] X. Wang, Q. Li, Z. Liu, J. Zhang, Z. Liu, R. Wang, Low-temperature growth and properties of ZnO nanowires, Appl. Phys. Lett. 84 (2004) 4941–4943.
[42] Y. Huang, M. Liu, Z. Li, Y. Zeng, S. Liu, Raman spectroscopy study of ZnO-based ceramic films fabricated by novel sol-gel process, Mater. Sci. Eng. B 97 (2003) 111–116.
[43] H.Y. He, J. Fei, J. Lu, Sm-doping effect on optical and electrical properties of ZnO films, J. Nanostruct. Chem. 5 (2015) 169–175.
[44] M. Ferhat, A. Zaoui, R. Ahuja, Magnetism and band gap narrowing in Cu-doped ZnO, Appl. Phys. Lett. 94 (1–3) (2009) 142502.
[45] M. Shakir, Mohd. Faraz, Mohd. Asif Sherwani, S.I. Al-Resayes, Photocatalytic degradation of the Paracetamol drug using Lanthanum doped ZnO nanoparticles and their in-vitro cytotoxicity assay, J. Lumin 76 (2016) 159–167.
[46] Y.P. Du, Y.W. Zhang, L.D. Sun, C.H. Yan, Efficient energy transfer in monodisperse Eu-doped ZnO nanocrystals synthesized from metal acetylacetonates in high-boiling solvents, J. Phys. Chem. C 112 (2008) 12234–12241.
[47] H. Akazawaa, H. Shinojima, Energy transfer and dissipation processes studied using photoluminescence of Eu^{3+} ions doped in epitaxial ZnO films, Thin Solid Films 616 (2016) 204–212.
[48] L.F. Koaoa, B.F. Dejenea, H.C. Swartb, S.V. Motloungc, T.E. Motaung, Characterization of annealed Eu^{3+}-doped ZnO flower-like morphology synthesized by chemical bath deposition method, Opt. Mater. 60 (2016) 294–304.
[49] D.D. Wang, G.Z. Xing, J.H. Yang, L.L. Yang, M. Gao, J. Cao, Y.J. Zhang, B. Yao, Dependence of energy transfer and photoluminescence on tailored defects in Eu-doped ZnO nanosheets-based microflowers, J. Alloy. Compd. 504 (2010) 22–26.